

## Formation of Mesoporous BaSO<sub>4</sub> Microspheres with a Larger Pore Size via Ostwald Ripening at Room Temperature

Qingde Chen and Xinghai Shen\*

Beijing National Laboratory for Molecular Sciences, Radiochemistry and Radiation Chemistry  
Key Laboratory of Fundamental Science, College of Chemistry and Molecular Engineering,  
Peking University, Beijing 100871, P. R. China

Received March 8, 2010; Revised Manuscript Received July 4, 2010

**ABSTRACT:** Mesoporous microspheres with a larger pore size (diameter of pore: ca. 35 nm, Barrett–Emmett–Teller (BET) surface area: 25.6 m<sup>2</sup>/g), the radial arrangement of irregular BaSO<sub>4</sub> nanorods, were successfully synthesized by the radiolysis of an aqueous solution of K<sub>2</sub>S<sub>2</sub>O<sub>8</sub>, Ba(NO<sub>3</sub>)<sub>2</sub>, and disodium ethylenediaminetetraacetate with an irradiation time of 1000 min (dose rate: 20 Gy/min) at room temperature. It was confirmed that the mesoporous microspheres with a larger pore size evolved from the mesoporous microspheres with a smaller pore size (diameter of pore: ca. 4 nm, BET surface area: 49.6 m<sup>2</sup>/g), which were generated at the early stage of the irradiation course and were mainly constructed by quasi-spherical nanoparticles, via Ostwald ripening at room temperature.

In the current materials synthesis and nanodevice fabrication, complex architectures constructed by the self-assembly and highly ordered organization of one- and two-dimensional (1D, 2D) nano-scale building blocks have been of intense interest because of their unique properties and potential applications, and are of importance in understanding the regularity of self-assembly with artificial building blocks.<sup>1</sup> As a result of rapid advancements in synthetic strategies, highly organized 1D and 2D building blocks of metals,<sup>2</sup> metal oxides,<sup>1c,e,f,3</sup> organic–inorganic hybrid materials,<sup>1d</sup> minerals,<sup>1a,4</sup> and so on<sup>5</sup> have been synthesized. Among the numerous synthetic methods, Ostwald ripening is simple and powerful, and has been widely applied.<sup>1a,c,3d,e,4d,5</sup> However, as to the materials with very low equilibrium solubility over a wide range of pH values, the molecular redissolution–crystallization events are suppressed to a great extent.<sup>1a</sup> This makes it difficult to construct the complex nanostructures based on these materials by Ostwald ripening. Therefore, it becomes necessary to extend the application range of Ostwald ripening in the construction of complex architectures. Furthermore, if this process takes place with a relatively rapid rate at room temperature, it will be more practical.

Barium sulfate (BaSO<sub>4</sub>), which is commonly known as Barite and inert in many chemical reactions, has been widely used in many areas such as catalyst carriers,<sup>6</sup> adsorbents,<sup>7</sup> contrast agents in the field of radiology,<sup>8</sup> fillers and additives in polymers,<sup>9</sup> and so forth.<sup>10</sup> Besides, BaSO<sub>4</sub> has been extensively used to investigate the precipitation and crystallization processes.<sup>1a,11</sup> So far, many amazing BaSO<sub>4</sub> particles with complex architectures have been synthesized, for example, fiber bundles/zones,<sup>12</sup> shuttlecocks,<sup>12b</sup> flowers,<sup>12b</sup> peanuts,<sup>13</sup> peaches,<sup>13</sup> etc. As one of the typical materials with a very low equilibrium solubility over a wide range of pH values, complex BaSO<sub>4</sub> nanostructures were seldom constructed by Ostwald ripening. Consequently, there still remains a great challenge.

In recent years, porous materials, especially mesoporous materials, have attracted much attention for their large specific surface area, tailored pore size and structure, surface properties, and therefore their wide range of potential applications in catalysis, adsorption, and so on.<sup>14</sup> As to BaSO<sub>4</sub>, after Li et al.<sup>6a</sup> reported the excellent performance of the agglomerate BaSO<sub>4</sub> nanotubes in supporting sulfates for methane activation at lower temperature, mesoporous BaSO<sub>4</sub> nanomaterials began to attract notice.<sup>6b,c,7a,15</sup> It is believed that mesoporous BaSO<sub>4</sub>

nanomaterials will be widely used in the future. Obviously, the syntheses of mesoporous BaSO<sub>4</sub> nanomaterials with different morphologies and controllable pore size are important and necessary. To the best of our knowledge, there is no report on the preparation of mesoporous BaSO<sub>4</sub> microsphere with a larger pore size.

$\gamma$ -Irradiation is a powerful method in the syntheses of nanoparticles and inorganic–polymer nanocomposites.<sup>16</sup> In our previous work, for the first time, we successfully synthesized BaSO<sub>4</sub> nanoparticles by the controlled-release effect of  $\gamma$ -irradiation, which subsequently formed “solid” microspheres via aggregation.<sup>17</sup> Herein, we report the radiolytic synthesis of mesoporous BaSO<sub>4</sub> microspheres with a larger pore size, the radial assemblies of irregular nanorods, in aqueous solution. As far as we know, this is the first report about this kind of complex BaSO<sub>4</sub> nanostructure. The research results indicate that Ostwald ripening can be effectively used to construct the complex nanostructures of the materials with very low equilibrium solubility over a wide range of pH values.

The typical aqueous solution containing 4 mmol/L Ba(NO<sub>3</sub>)<sub>2</sub>, 4 mmol/L K<sub>2</sub>S<sub>2</sub>O<sub>8</sub>, and 8 mmol/L disodium ethylenediaminetetraacetate (EDTA) was prepared. After being bubbled with high-purity N<sub>2</sub> under anaerobic conditions, the solution was irradiated in the field of a <sup>60</sup>Co  $\gamma$ -ray source for a definite time at the location whose dose rate was fixed at 20 Gy/min. Then, white precipitates were obtained. Morphology of the products was observed with a scanning electron microscope (SEM, Hitachi S-4800), a transmission electron microscope (TEM, JEOL JEM-200CX), and a high-resolution TEM (HRTEM, Hitachi 9000). To investigate the inner structure, the obtained powder was dispersed in water and sonicated at room temperature for 1 h to get the sample for characterization. X-ray diffraction (XRD) pattern was recorded on an X'Pert PRO MPD diffractometer with Cu K $\alpha$  radiation, X-ray photoelectron spectrum (XPS) was collected on a Kratos Axis Ultra spectrometer with monochromatized Al K $\alpha$  radiation, and N<sub>2</sub> adsorption–desorption isotherms were determined on a Micromeritics ASAP-2010 apparatus.

As is well-known, when the diluted aqueous solution is irradiated by  $\gamma$ -rays, the water molecules absorb the irradiation energy and generate many reactive species, such as e<sub>aq</sub><sup>-</sup>, H, and •OH (eq 1):<sup>18</sup>



Then, the oxidative •OH is eliminated by EDTA, with a rate constant of 4.0 × 10<sup>8</sup> L · mol<sup>-1</sup> · s<sup>-1</sup>,<sup>18</sup> and the reducing species,

\*Corresponding author. Fax: +86-10-62759191. Tel: +86-10-62765915. E-mail: xshen@pku.edu.cn.

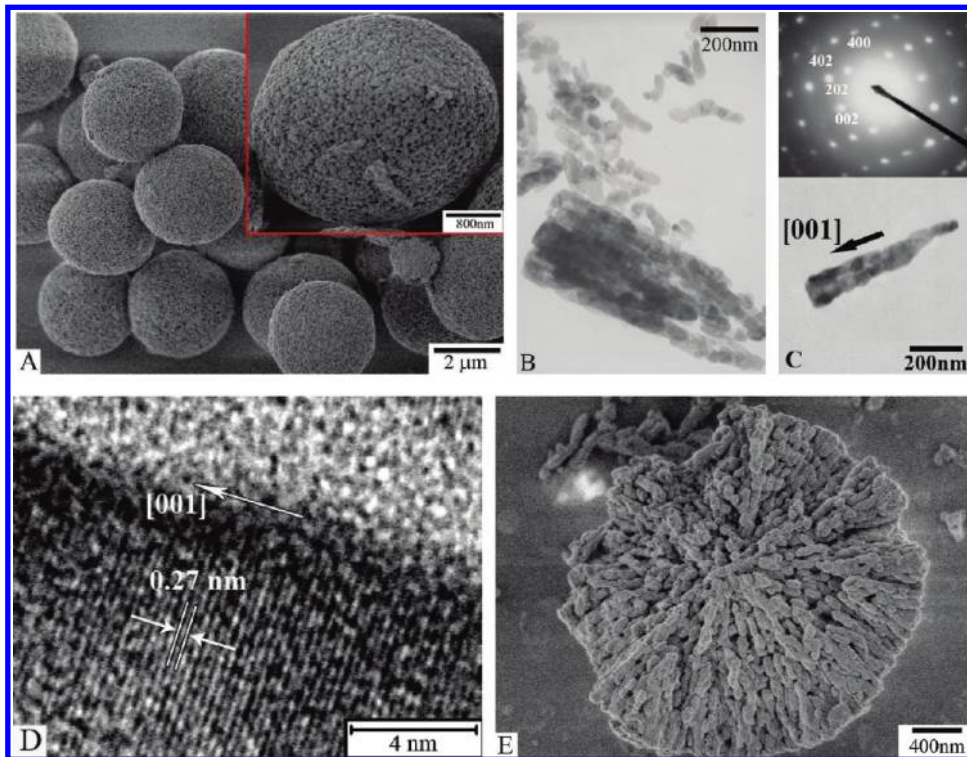


**Figure 1.** SEM images (A and E), TEM images (B and C), and HRTEM image (D) of the sample synthesized at an irradiation time of 1000 min. The insets in (A) and (C) show the image at higher magnification and the SAED pattern of the corresponding product, respectively. The dose rate is 20 Gy/min, and the concentration of EDTA is 8 mmol/L.

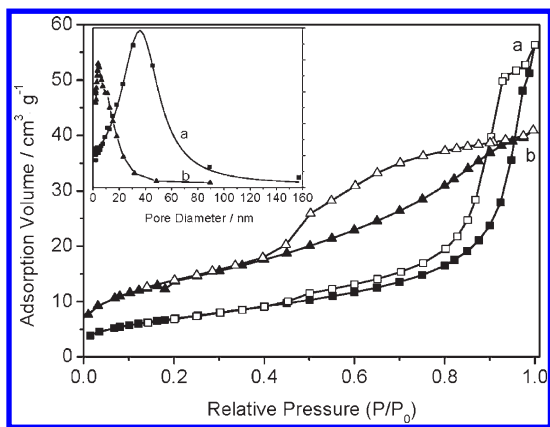
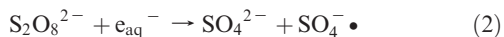


**Figure 2.** N<sub>2</sub> adsorption (solid)—desorption (open) isotherms of the samples synthesized at different irradiation times: (a) 1000 min, (b) 250 min. The inset shows the pore size distribution of the corresponding samples. The dose rate is 20 Gy/min, and the concentration of EDTA is 8 mmol/L.

especially e<sub>aq</sub><sup>-</sup>, reduce S<sub>2</sub>O<sub>8</sub><sup>2-</sup> ions to SO<sub>4</sub><sup>2-</sup> ions (eq 2), with a rate constant of 1.2 × 10<sup>10</sup> L · mol<sup>-1</sup> · s<sup>-1</sup>.<sup>18</sup>



Thus, the controlled release of SO<sub>4</sub><sup>2-</sup> and the following generation of BaSO<sub>4</sub> could be realized, which favors the generation of uniform BaSO<sub>4</sub> microspheres.<sup>17</sup>

Figure 1A presents the SEM image of the sample prepared at an irradiation time of 1000 min. It can be seen that the product is composed of microspheres with a diameter of 2–4 μm, besides a few fragments. From the related SEM image in higher magnification (inset, Figure 1A), it can be clearly found that a lot of pores, with a diameter ranging from 20 to 60 nm, are evenly distributed on the surface of the microspheres. Moreover, in the N<sub>2</sub>

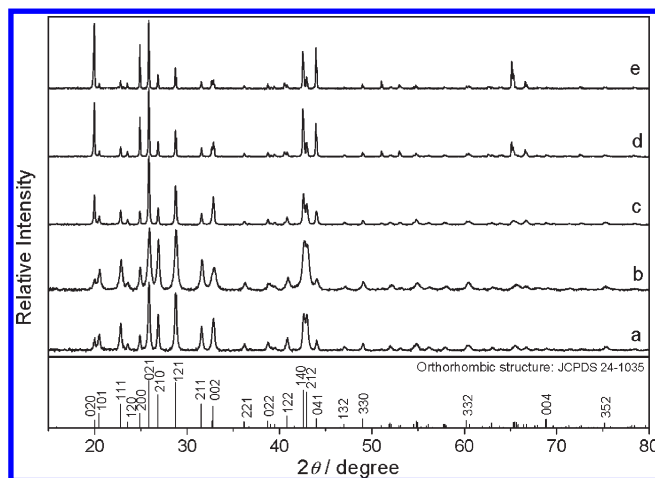


**Figure 3.** XRD patterns of the samples synthesized under different conditions: (a) irradiation time: 1000 min, [EDTA] = 8 mmol/L; (b) irradiation time: 250 min, [EDTA] = 8 mmol/L; (c) irradiation time: 1000 min, [EDTA] = 0.8 mmol/L; (d) irradiation time: 1000 min, [EDTA] = 0.08 mmol/L; (e) irradiation time: 1000 min, [EDTA] = 0. The dose rate is 20 Gy/min.

adsorption–desorption isotherm experiment, there appears an obvious hysteresis loop (curve a, Figure 2) associated with the filling of the mesopores due to capillary condensation, and the Barrett–Emmett–Teller (BET) surface area is calculated to be 25.6 m<sup>2</sup>/g, which is large for high-density materials.<sup>1f</sup> Furthermore, the pore size profile of the sample (curve a, inset of Figure 2) shows that most of the pores are mesoporous and there is a single peak at about 35 nm, which is consistent with the SEM result. All of the above results indicate the existence of a mesoporous structure with a larger pore size in the microspheres.

The corresponding XPS analysis (Figure SI-1, Supporting Information) shows that the binding energies of Ba 3d, S 2p,

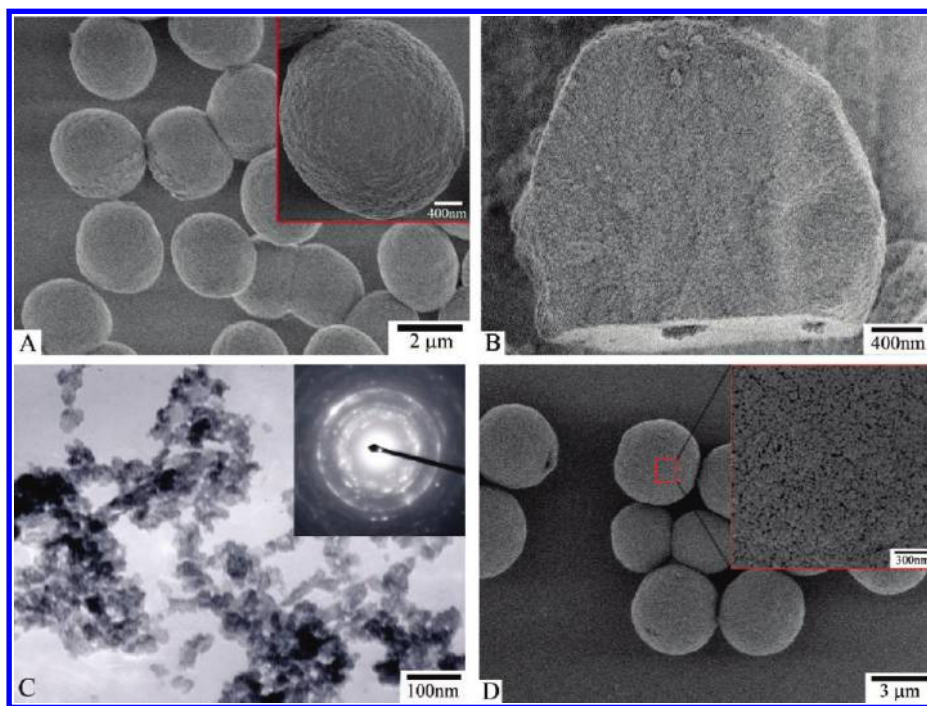


**Figure 4.** SEM (A, B, D) and TEM (C) images of the samples synthesized at different irradiation times: (A–C) 250 min, (D) 450 min. Insets: (A and D) the image of the corresponding product at higher magnification; (C) the SAED pattern of the corresponding product. The dose rate is 20 Gy/min, and the concentration of EDTA is 8 mmol/L.

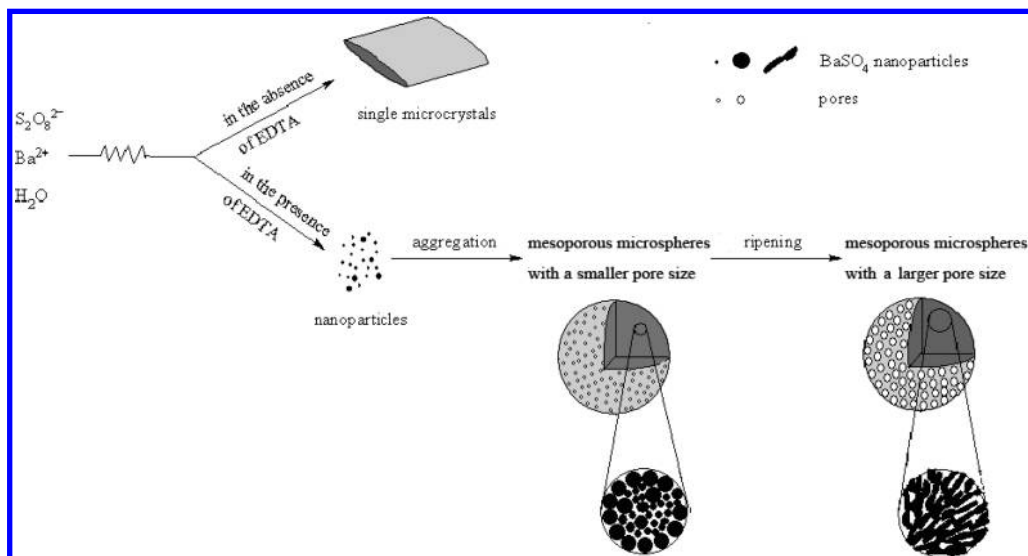
and O 1s are 779.76, 168.40, and 531.18 eV, respectively, close to the values of  $\text{BaSO}_4$  reported in the literature.<sup>19</sup> Furthermore, the analysis result suggests the presence of Ba, S, and O in a ratio of 1.00:0.95:4.02, close to the stoichiometry of  $\text{BaSO}_4$  within experimental error. Thus, the generation of  $\text{BaSO}_4$  can be demonstrated. The related XRD pattern (curve a, Figure 3), which is consistent with the orthorhombic  $\text{BaSO}_4$  structure, further confirms the generation of  $\text{BaSO}_4$ .

The TEM images of the fragments presented in Figure 1B,C clearly show that the mesoporous microspheres with a larger pore size are constructed by numerous irregular nanorods with a diameter ranging from 40 to 120 nm. This is further confirmed by the SEM image of the cross-section of a microsphere (Figure 1E). Moreover, the SEM image (Figure 1E) shows that the microspheres are formed via the radial self-assembly of the irregular nanorods, and there are interstitial spaces available among these nanorods, which provide connected channels for mass exchange between the inner space of  $\text{BaSO}_4$  microspheres and the outer solution. The selected area electron diffraction (SAED) pattern related to a small fragment (inset, Figure 1C) can be indexed to the [010] zone axis of orthorhombic  $\text{BaSO}_4$ , suggesting that a single nanorod is a single crystal of predominantly grown along the [001] direction. The typical HRTEM image of a nanorod shown in Figure 1D exhibits clear lattice fringes with  $d$  spacing of 0.27 nm, which corresponds to (002) reflection of orthorhombic  $\text{BaSO}_4$ , further confirming that the nanorods are single crystals grown along the  $c$ -axis. However, the alignment of the rodlike nanocrystals is not parallel, and there is a certain angle between them (Figure 1B,C), leading to the radial arrangement of the nanorods. It is the arrangement mode and the irregular shape that causes the generation of the mesoporous structure with a larger pore size.

In the syntheses of  $\text{BaSO}_4$  particles, amino-carboxylate additives play important roles.<sup>11c–h,12f,20</sup> As one of the important amino-carboxylate additives, EDTA is found to affect the morphology of  $\text{BaSO}_4$  particles in this work. In the absence of EDTA, the obtained product is made of well-crystallized Barite crystals according to the XRD analysis (curve e, Figure 3). The TEM

image (Figure SI-2A, Supporting Information) shows that the product is composed of rectangular tablets with different sizes. The SAED analysis of the edge of a particle (inset, Figure SI-2A, Supporting Information) indicates that the obtained particles are single-crystal Barite. The SEM image (Figure SI-2B, Supporting Information) further shows that the crystals are pillow-like, similar to the shape reported in the literature.<sup>11e,h</sup> When the concentration of EDTA increases, the obtained  $\text{BaSO}_4$  particles are gradually transformed from pillow shape to microsphere, from single crystals to the aggregation of nanorods, and from nonporous to mesoporous (Figures 1A and SI-2B–D, Supporting Information). At the same time, the XRD diffraction peaks are broadened with an increase in the concentration of EDTA (curves a and c–e, Figure 3), suggesting that the building blocks of the Barite particles become small gradually. In the literature, because of a lower concentration and narrower concentration range of EDTA, similar morphology transformation was not found, while at the higher concentration of EDTA (ca. 8 mmol/L), quasi-spherical nanoparticles with an average size of 16 nm were obtained.<sup>20</sup> The generation of nanoparticles was ascribed to the adsorption of EDTA on the surface of  $\text{BaSO}_4$  nuclei, which retards the growth of  $\text{BaSO}_4$  nuclei and favors the formation of nanoparticles.<sup>20</sup> Herein, the formation of  $\text{BaSO}_4$  nanoparticles, which subsequently form microspheres via aggregation, may be due to a similar reason. Recently, we obtained  $\text{BaSO}_4$  microspheres with a diameter of ca. 700 nm via increasing the pH value, leading to a stronger interaction between  $\text{Ba}^{2+}$  and EDTA. It can be seen that EDTA plays an important role in the formation of  $\text{BaSO}_4$  microspheres.

Besides EDTA, the irradiation time could also affect the morphology of the  $\text{BaSO}_4$  microspheres. In the present work, the dose rate was fixed at 20 Gy/min. At an irradiation time of 250 min, microspheres were formed (Figure 4A). From the morphologies of the surface (inset, Figure 4A) and the cross-section (Figure 4B) of some microspheres, it seems that they are “solid”. The TEM image of the fragments and the related SAED analysis (Figure 4C) indicate that the obtained microspheres consist of well-crystallized quasi-spherical nanoparticles. Nevertheless, the results of  $\text{N}_2$

Scheme 1. Growth Mechanism of Mesoporous BaSO<sub>4</sub> Microspheres with a Larger Pore Size

adsorption–desorption isotherm experiments (curves b, Figure 2) suggest that the microspheres are actually mesoporous, but the diameter of the pores is only about 4 nm, which is much smaller than that at an irradiation time of 1000 min and not easy to be found by SEM. The BET surface area is calculated to be 49.6 m<sup>2</sup>/g, which is appreciably larger than that at an irradiation time of 1000 min. This implies that the size of the building block of the former is smaller than that of the latter. The widths of the XRD diffraction peaks are obviously larger than those at the irradiation time of 1000 min (curves a and b, Figure 3), also suggesting that the size of nanoparticles increases by increasing the irradiation time. This is consistent with the analysis result of the BET surface area. The visual proof comes from the analysis of the fragments, which shows that the size of the building block of the mesoporous microspheres with a smaller pore size (Figure 4C) is obviously smaller than that at an irradiation time of 1000 min (Figure 1B,C). When the irradiation time increases to 450 min, there appears to be an obvious porous structure, with a pore diameter of about 10 nm, on the surface of most microspheres (Figure 4D).

Thus, it can be concluded that the mesoporous BaSO<sub>4</sub> microspheres with a larger pore size should evolve from the mesoporous microspheres with a smaller pore size. In the evolution process, the quasi-spherical nanoparticles (the building block of the mesoporous microspheres with a smaller pore size) were transformed to the nanorods (the building block of the mesoporous microspheres with a larger pore size). This evolution may be the result of ripening, etching, or  $\gamma$ -ray action. To clarify the evolution pathway, the water-washed mesoporous microspheres with a smaller pore size (irradiation time: 250 min) were dispersed in water and irradiated for 1000 min (dose rate: 20 Gy/min). There is no obvious mesoporous structure with a larger pore size on the surface of most microspheres (not shown here). In addition, during the irradiation course, the size of the BaSO<sub>4</sub> nanoparticles became larger. This cannot be ascribed to the action of etching only. Therefore, the ripening of BaSO<sub>4</sub> nanoparticles should play a key role in the formation of mesoporous structure with a larger pore size.

To confirm our surmise, the mesoporous BaSO<sub>4</sub> microspheres with a smaller pore size obtained at an irradiation time of 250 min were ripened in the irradiated mother solution. The SEM images of the microspheres and cross-section of a microsphere (Figure SI-3, Supporting Information) clearly show that the mesoporous microspheres with a smaller pore size are transformed to mesoporous ones with a larger pore size, similar to that obtained at the irradiation time of 1000 min (Figure 1A). In other words, the reconstruction of BaSO<sub>4</sub> microspheres can be easily realized via a simple

ripening process. Therefore, if the conditions are suitable, Ostwald ripening can be effectively used to construct complex BaSO<sub>4</sub> nanostructures with a relatively rapid rate at room temperature, and it makes the process more practical. As to the specific species leading to the morphology transformation, it is worthy of further investigation.

In summary, the mesoporous BaSO<sub>4</sub> microspheres with a larger pore size are successfully synthesized by  $\gamma$ -irradiation. Indeed, the formation process can be divided into two steps as follows (Scheme 1).

- (1) When the aqueous solution containing S<sub>2</sub>O<sub>8</sub><sup>2-</sup> and Ba<sup>2+</sup> ions is irradiated under anaerobic conditions, Ba<sup>2+</sup> ions are precipitated by the control-released SO<sub>4</sub><sup>2-</sup> ions, leading to the formation of BaSO<sub>4</sub> nanoparticles in the presence of EDTA, which are subsequently aggregated to form microspheres, while pillow-like BaSO<sub>4</sub> microcrystals are generated in the absence of EDTA. In this step, the concentration of EDTA and the controlled release of SO<sub>4</sub><sup>2-</sup> ions are important to the formation of the microspheres.
- (2) At the early stage of the irradiation course, the obtained microspheres are mainly constructed by quasi-spherical nanoparticles and have a mesoporous structure with a smaller pore size. Because a smaller nanoparticle has a higher surface energy, a part of the BaSO<sub>4</sub> nanoparticles, especially the smaller, may be gradually dissolved in the course of irradiation, resulting in a higher solubility of BaSO<sub>4</sub>. Then, BaSO<sub>4</sub> is precipitated on the surfaces of the larger nanoparticles again, and a new redissolution–crystallization balance can be achieved. Indeed, this is an Ostwald ripening process. In the process, some species may preferentially adsorb on the surfaces parallel to the [001] axes of BaSO<sub>4</sub> nanoparticles, leading to the formation of irregular nanorods. The radial arrangement and the irregular shape cause the generation of the mesoporous structure with a larger pore size. Obviously, Ostwald ripening can be effectively used to construct complex BaSO<sub>4</sub> nanostructures with a relatively rapid rate at room temperature.

It is believed that the result reported herein will be helpful in constructing complex nanostructures. Because BaSO<sub>4</sub> is inert in

many chemical reactions and a large pore size favors the mass exchange, mesoporous BaSO<sub>4</sub> microspheres with a larger pore size may act as promising candidates for catalyst carrier, adsorbents, and so on.

**Acknowledgment.** This work was supported by the National Natural Science Foundation of China (Grant 20871009) and the Coordinated Research Projects of International Atomic Energy Agency (Research Contract No. 15107).

**Supporting Information Available:** X-ray photoelectron spectrum; TEM and SEM images. This material is available free of charge via the Internet at <http://pubs.acs.org>.

## References

- (1) (a) Meldrum, F. C.; Colfen, H. *Chem. Rev.* **2008**, *108*, 4332. (b) Mann, S. *Nat. Mater.* **2009**, *8*, 781. (c) Zeng, H. C. *J. Mater. Chem.* **2006**, *16*, 649. (d) Park, S.; Lim, J. H.; Chung, S. W.; Mirkin, C. A. *Science* **2004**, *303*, 348. (e) Cao, A. M.; Hu, J. S.; Liang, H. P.; Wan, L. J. *Angew. Chem.-Int. Ed.* **2005**, *44*, 4391. (f) Zhong, L. S.; Hu, J. S.; Liang, H. P.; Cao, A. M.; Song, W. G.; Wan, L. J. *Adv. Mater.* **2006**, *18*, 2426.
- (2) Yang, J. H.; Qi, L. M.; Lu, C. H.; Ma, J. M.; Cheng, H. M. *Angew. Chem.-Int. Ed.* **2005**, *44*, 598.
- (3) (a) Uchiyama, H.; Imai, H. *Cryst. Growth Des.* **2007**, *7*, 841. (b) Li, Z. H.; Gessner, A.; Richters, J. P.; Kalden, J.; Voss, T.; Kubel, C.; Taubert, A. *Adv. Mater.* **2008**, *20*, 1279. (c) Park, G. S.; Shindo, D.; Waseda, Y.; Sugimoto, T. *J. Colloid Interface Sci.* **1996**, *177*, 198. (d) Yang, H. G.; Zeng, H. C. *J. Phys. Chem. B* **2004**, *108*, 3492. (e) Zhang, S. D.; Li, Y. M.; Wu, C. Z.; Zheng, F.; Xie, Y. *J. Phys. Chem. C* **2009**, *113*, 15058.
- (4) (a) Walsh, D.; Mann, S. *Nature* **1995**, *377*, 320. (b) Voinescu, A. E.; Kellermeier, M.; Bartel, B.; Carnerup, A. M.; Larsson, A. K.; Touraud, D.; Kunz, W.; Kienle, L.; Pfitzner, A.; Hyde, S. T. *Cryst. Growth Des.* **2008**, *8*, 1515. (c) Garcia-Ruiz, J. M.; Meler-Garcia, E.; Hyde, S. T. *Science* **2009**, *323*, 362. (d) Chen, Q. D.; Bao, H. Y.; Shen, X. H. *Phase Transit.* **2008**, *81*, 591.
- (5) (a) Ito, T.; Inumaru, K.; Misono, M. *Chem. Mater.* **2001**, *13*, 824. (b) Ito, T.; Song, I. K.; Inumaru, K.; Misono, M. *Chem. Lett.* **1997**, 727.
- (6) (a) Li, F. B.; Yuan, G. Q. *Chem. Commun.* **2005**, 2238. (b) Li, F. B.; Yuan, G. Q. *J. Catal.* **2006**, *239*, 282. (c) Nagaraja, B. M.; Jung, K. D.; Ahn, B. S.; Abimanyu, H.; Yoo, K. S. *Ind. Eng. Chem. Res.* **2009**, *48*, 1451. (d) Andrade, L. H.; Silva, A. V.; Pedrozo, E. C. *Tetrahedron Lett.* **2009**, *50*, 4331.
- (7) (a) Lin, J.; Gao, H. W. *J. Mater. Chem.* **2009**, *19*, 3598. (b) Gao, H. W.; Lin, J.; Li, W. Y.; Hu, Z. J.; Zhang, Y. L. *Environ. Sci. Pollut. Res.* **2010**, *17*, 78.
- (8) O'Connor, S. D.; Summers, R. M. *Acad. Radiol.* **2007**, *14*, 72.
- (9) (a) Qu, M. H.; Wang, Y. Z.; Wang, C.; Ge, X. G.; Wang, D. Y.; Zhou, Q. *Eur. Polym. J.* **2005**, *41*, 2569. (b) Ricker, A.; Liu-Snyder, P.; Webster, T. J. *Int. J. Nanomed.* **2008**, *3*, 125. (c) Yao, C. G.; Yang, G. S. *Polym. Adv. Technol.* **2009**, *20*, 768.
- (10) (a) Heinrichs, U.; Blume, A.; Bussmann, N.; Engels, R.; Kemmerling, G.; Weber, S.; Ziemons, K. *Nucl. Instrum. Methods Phys. Res., Sect. A* **2002**, *486*, 60. (b) Salah, N.; Habib, S. S.; Khan, Z. H.; Al-Hamed, S.; Lochab, S. P. *J. Lumin.* **2009**, *129*, 192. (c) Manam, J.; Das, S. J. *Alloys Compd.* **2010**, *489*, 84.
- (11) (a) Judat, B.; Kind, M. *J. Colloid Interface Sci.* **2004**, *269*, 341. (b) Coveney, P. V.; Davey, R.; Griffin, J. L. W.; He, Y.; Hamlin, J. D.; Stackhouse, S.; Whiting, A. *J. Am. Chem. Soc.* **2000**, *122*, 11557. (c) Piana, S.; Jones, F.; Gale, J. D. *CrystEngComm* **2007**, *9*, 1187. (d) Jones, F.; Richmond, W. R.; Rohl, A. L. *J. Phys. Chem. B* **2006**, *110*, 7414. (e) Jones, F.; Oliveira, A.; Rohl, A. L.; Ogden, M. I.; Parkinson, G. M. *CrystEngComm* **2006**, *8*, 869. (f) Uchida, M.; Sue, A.; Yoshioka, T.; Okuwaki, A. *CrystEngComm* **2001**, *5*, 1. (g) Uchida, M.; Sue, A.; Yoshioka, T.; Okuwaki, A. *J. Mater. Sci. Lett.* **2000**, *19*, 1373. (h) Jones, F.; Jones, P.; Ogden, M. I.; Richmond, W. R.; Rohl, A. L.; Saunders, M. *J. Colloid Interface Sci.* **2007**, *316*, 553.
- (12) (a) Wang, T. X.; Reinecke, A.; Colfen, H. *Langmuir* **2006**, *22*, 8986. (b) Li, M.; Colfen, H.; Mann, S. *J. Mater. Chem.* **2004**, *14*, 2269. (c) Yu, S. H.; Antonietti, M.; Colfen, H.; Hartmann, J. *Nano Lett.* **2003**, *3*, 379. (d) Li, M.; Mann, S. *Langmuir* **2000**, *16*, 7088. (e) Qi, L. M.; Colfen, H.; Antonietti, M.; Li, M.; Hopwood, J. D.; Ashley, A. J.; Mann, S. *Chem.-Eur. J.* **2001**, *7*, 3526. (f) Romero-Ibarra, I. C.; Rodriguez-Gattorno, G.; Garcia-Sanchez, M. F.; Sanchez-Solis, A.; Manero, O. *Langmuir* **2010**, *26*, 6954.
- (13) Qi, L. M.; Colfen, H.; Antonietti, M. *Chem. Mater.* **2000**, *12*, 2392.
- (14) (a) Lu, A. H.; Schuth, F. *Adv. Mater.* **2006**, *18*, 1793. (b) Hoa, M. L. K.; Lu, M. H.; Zhang, Y. *Adv. Colloid Interface Sci.* **2006**, *121*, 9. (c) Frenzer, G.; Maier, W. F. *Ann. Rev. Mater. Res.* **2006**, *36*, 281. (d) Barton, T. J.; Bull, L. M.; Klemperer, W. G.; Loy, D. A.; McEnaney, B.; Misono, M.; Monson, P. A.; Pez, G.; Scherer, G. W.; Vartuli, J. C.; Yaghi, O. M. *Chem. Mater.* **1999**, *11*, 2633. (e) Lai, M.; Riley, D. J. *J. Colloid Interface Sci.* **2008**, *323*, 203.
- (15) Nagaraja, B. M.; Abimanyu, H.; Jung, K. D.; Yoo, K. S. *J. Colloid Interface Sci.* **2007**, *316*, 645.
- (16) (a) Chen, Q. D.; Shen, X. H.; Gao, H. C. *Adv. Colloid Interface Sci.* **2010**, *159*, 32. (b) Belloni, J. *Catal. Today* **2004**, *113*, 141. (c) Reddy, K. R.; Lee, K. P.; Gopalan, A. I.; Kim, M. S.; Showkat, A. M.; Nho, Y. C. *J. Polym. Sci., Polym. Chem.* **2006**, *44*, 3355. (d) Kuo, S. W.; Chung, Y. C.; Jeong, K. U.; Chang, F. C. *J. Phys. Chem. C* **2008**, *112*, 16470.
- (17) Chen, Q. D.; Bao, H. Y.; Shen, X. H. *Radiat. Phys. Chem.* **2008**, *77*, 974.
- (18) Buxton, G. V.; Greenstock, C. L.; Helman, W. P.; Ross, A. B. *J. Phys. Chem. Ref. Data* **1988**, *17*, 513.
- (19) Moulder, J. F.; Stickle, W. F.; Sobol, P. E.; Bomben, K. D. In *Handbook of X-ray Photoelectron Spectroscopy*; Perkin Elmer Physical Electronics Division: Eden, 1992.
- (20) Zhao, Y. H.; Liu, J. R. *Chem. Lett.* **2006**, *35*, 1040.